# Three-Dimensional Description of Pulmonary Deposition of Inhaled Aerosol Using Data from Multimodality Imaging

John S. Fleming, Peter Halson, Joy Conway, Elizabeth Moore, Michael A. Nassim, Adel H. Hashish, Adrian G. Bailey, Stephen T. Holgate and Theodore B. Martonen

*Department of Medical Physics and University Department of Medicine, Southampton General Hospital, Southampton; Department of Electrical Engineering, Southampton University, Southampton; Clinical Pharmacology, Fisons plc, Loughborough; and Health Effects Research Laboratory, U.S. Environmental Protection Agency, Research Triangle Park, NC*

Three-dimensional assessment of pulmonary deposition of inhaled aerosol may be performed using SPECT. The use of aligned anatomical images enables improved accuracy of quantification and anatomical localization of deposition. **Methods:** Techniques of analyzing these data and their application to deposition studies of two nebulizer-generated aerosols (mass median diameters 1.5 and 6.5 $\mu$m, respectively) in 12 normal subjects are described. The deposition data were transformed to a standard hemispherical shape and the mean distribution pattern for each aerosol evaluated. Deposition by airway generation was then calculated using a spatial model of airway morphology. The results were compared to those from planar image analysis. **Results:** The hemispherical transform yielded considerably more qualitative information on deposition pattern. The central-to-peripheral concentration ratio between conducting and alveolated airways was 5.27 for the coarser aerosol and 2.43 for the fine. The two-dimensional spatial estimates of the ratio were 2.61 and 2.03 respectively. **Conclusion:** Analysis of multimodality imaging data considerably enhanced information on deposition compared to planar imaging. It provides new data on aerosol deposition which will be of value to physicians involved in drug inhalation therapy.

**Key Words:** aerosol deposition measurement; three-dimensional analysis; multimodality imaging

**J Nucl Med 1996; 37:873–877**

Measurement of pulmonary deposition of inhaled aerosol is important in studies on drug inhalation therapy and health effects of atmospheric particulate pollutants. Radionuclide imaging has been extensively used to measure both total lung deposition and its spatial distribution (*1*). Planar imaging provides only a two-dimensional projection of the underlying three-dimensional distribution, which limits its ability to assess deposition patterns. This can be overcome using SPECT which provides a three-dimensional distribution (*2,3*). The use of aligned anatomical information from either CT or MRI provides both a map of attenuation coefficients of the thorax enabling increased accuracy of measurement and the opportunity to relate radionuclide deposition to lung anatomy (*3*). The data may be transformed to a standard hemispherical shape which allows the spatial distribution of deposition on groups of similar subjects to be averaged and the image pattern of the group as a whole to be defined.

This process, however, still only analyzes the spatial distribution of deposition, and the data are therefore not in the form ideally required by medical practitioners interested in pulmonary deposition patterns of drug or by lung modelers seeking validation of their models in practical measurements in human subjects. Both groups require description of deposition in relation to the airway tree. This consists of a branching structure of airways which become successively narrower and more numerous with subsequent branches. In the most widely accepted model of the airway tree, the Weibel model (*4*), the airways at a particular level of branching and therefore of a similar diameter are described as being of a particular generation. The transformation of the deposition distribution from the spatial to airway generation frame of reference requires knowledge of the three-dimensional distribution of the airway network. If the Weibel model with certain assumptions about branching angles is used, then a shape quite different from that of the real lungs is obtained (*5*). To overcome this limitation, a conceptual model has been developed based on the Weibel model describing the spatial distribution of the airways in relation to the hemispherical transform of the lung (*6*).

In this article, we describe: (a) the transformation of deposition data to the hemispherical model and methods of displaying and analyzing the transformed data both spatially and with respect to the airway tree and (b) the application of this analysis to measurements of inhaled aerosol from two different nebulizers in 12 normal subjects.

## METHODS

### Hemispherical Transformation of the Lung

The hemispherical shape was chosen as the standard transform because it was considered a good first-order model of the real lung. Although it only accounts for individual variation of shape in an approximate manner, it does provide information on penetration from the center to periphery of the lung, which is of particular interest in particle deposition measurements. The lung space is described in cartesian coordinates, using aligned anatomical data, with each voxel, V, described by x, y, z coordinates (Fig. 1). The center of the lung, O, at the origin is defined as the hilum of the lung where the main bronchus crosses the lung surface. For each voxel in the lung space (x, y, z), the straight line joining it to the center is extrapolated outwards until it meets the surface at point P ($x_p$, $y_p$, $z_p$). The fractional radial distance of the voxel (r′) is calculated as r/b, where r is the distance between the lung center and the voxel and b that between the center to the extrapolated peripheral point ($x_p$, $y_p$, $z_p$). Each voxel is then characterized first with respect to spherical coordinates by the fractional radial distance r′ and the two angles $\theta$ and $\phi$ and therefore to a new Cartesian coordinate system (x′, y′, z′) where

Received Mar. 1, 1995; revision accepted Aug. 25, 1995.

For correspondence or reprints contact: J.S. Fleming, PhD, Department of Nuclear Medicine, Southampton General Hospital, Southampton S016 6YD, U.K.

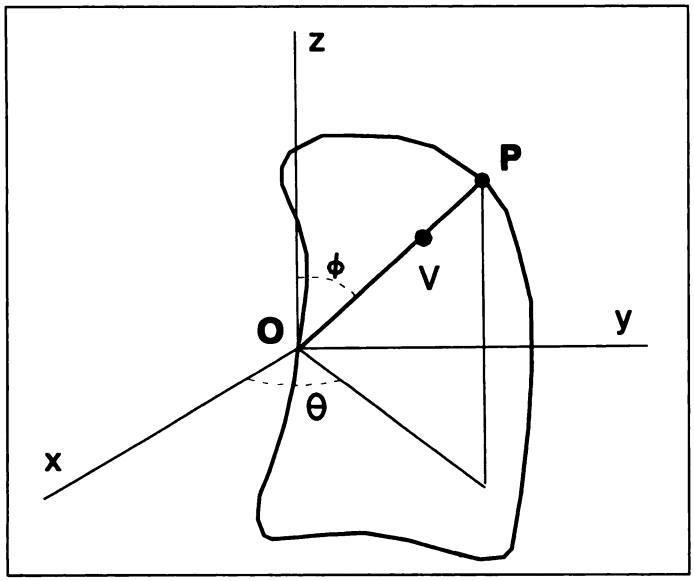


**FIGURE 1.** Schematic diagram of the process of the hemispherical transform. Each voxel, V, in the lung space is characterized by angles $\theta$ and $\phi$, and the fractional radial distance from the lung center to the corresponding point on the periphery OV/OP.

$$x' = x \cdot n/b \qquad \text{Eq. 1A}$$

$$y' = y \cdot n/b \qquad \text{Eq. 1B}$$

$$z' = z \cdot n/b, \qquad \text{Eq. 1C}$$

where n is the radius of the hemisphere in voxels. In this study, the transformed data were stored in a 64 × 64 × 64 matrix with the hemisphere being of radius 32 voxels. The images can then be displayed as a series of transverse slices with each image being of semicircular shape. To further summarize the data, coronal and transverse "polar" plots are constructed. The coronal polar matrix $C_{r'\phi}$ is calculated as:

$$c_{r'\phi} = \left( \sum_{\text{All voxels at } r'\phi} L_{xyz} \right) \Big/ n_{r'\phi}, \qquad \text{Eq. 2}$$

where $L_{xyz}$ represents the SPECT image distribution and $n_{r'\phi}$ the number of voxels at radius r′ and vertical angle $\phi$. The polar matrix is then converted to Cartesian coordinates as a two-dimensional polar plot which is a coronal view of the hemispherical data in which the contributions of all the voxels at each value of the fractional radial distance r′ and vertical angle $\phi$ are averaged. A similar transverse polar plot can be derived by performing the sum over all points with given values of r′ and $\theta$.

Additional condensation of the data can be achieved by summing the data at a particular fractional radial distance (i.e., within a particular hemispherical shell). In this study, the lung was split into ten shells.

An algorithm for hemispherically transforming right lung radionuclide image data and calculating the corresponding polar plots and shell data has been implemented on a Sun Sparcstation (Sun Microsystems, Mountain View, CA) computer as part of the PICS image processing package (*7*). The lung outlines may be obtained from segmentation of either CT or MR images.

### Imaging Procedures

Subjects inhaled a radiolabeled aerosol from a jet nebulizer using a controlled tidal breathing regime (*8*). The particle size distribution of the aerosol was measured using a Malvern particle analyzer (*9*). The nebulizer contained a suspension of $^{99m}$Tc-labeled albumin microspheres and the subject breathed until approximately 25 MBq were in the lungs. Four marks were placed at suitable positions on the subject's skin surface and on each a low activity $^{57}$Co source was placed. The accuracy of positioning was determined using measurements on markers which were known distances apart. SPECT imaging was then performed on a dual-head gamma camera using 64 projection images around 360°, each of 30 sec duration. A 128 × 128 matrix was used that corresponded to a pixel size of 0.47 cm. MR images of the thorax were also obtained on each subject. The positions of the skin marks were identified using castor oil capsules.

Both sets of images were transferred to the processing computer for analysis. The MR images were aligned to the SPECT imaging position using the marker positions (*10*). The algorithm provided estimates of the random error in alignment. They were then segmented into regions representing tissue, lung and bone to provide a map for attenuation correction in the SPECT reconstruction (*11*). Image segmentation was performed semiautomatically using the Analyze (Mayo Foundation, Rochester, MN) software system. The reconstruction algorithm included attenuation and scatter correction (*12*). The hemispherical transformation of the deposition data with respect to the lung space was performed on the right lung using the segmented MR image. The corresponding polar plots were formed and the total space volume of each shell i, $T_i$, and the total activity per shell, $s_i$, calculated. Misalignment effects were investigated in two subjects by shifting the MR images by a distance equal to the mean alignment error and re-analyzing the data. The hemispherical plots were compared qualitatively by visual inspection and the shell data quantitatively by calculating the effect on deposition concentration per shell. Planar imaging of the thorax was also performed to compare three-dimensional analysis with the conventional planar approach.

The relationship between site of deposition and density of the lung was studied in two male subjects. CT images were obtained as a series of twelve transverse slices covering the volume of the thorax on a Siemens Somatom DR2 (Siemens, Ehrlangen, Germany) imager and transferred to the Sun Sparcstation. They were interpolated to a full three-dimensional matrix and the hounsfield units were converted to density (*12*). The right lung volume was segmented semiautomatically and the point representing the center of the lung was defined manually. The data were then hemispherically transformed and the mean polar plots and shell data were calculated, which enabled us to obtain information on the spatial variation of density in the lung relative to the hemispherical shape.

### Transformation of Deposition Data from Shell to Generation Description

The transformation of deposition data from shell to generation description was achieved by use of a three-dimensional morphological model of the airways tree (*6*). This process used data from the Weibel model of the lung (*4*) and information on lung volume and density from CT and MR images to calculate the volume of each airway generation j present in each shell i, $V_{ij}$. The model assumed that the airway tree could be divided into the conducting airways, generations 1–14, and the acini, generations 15–23.

By assuming uniform deposition per generation, the following expression can be written for the total activity in each shell:

$$s_i = \sum_{j=1}^{23} V_{ij} \cdot g_j/G_j, \qquad \text{Eq. 3}$$

where $g_j$ and $G_j$ represent the activity and air volume of generation j. Further assumptions about the deposition pattern allowed this equation to be solved for the amount per generation. Details of this process are described elsewhere (*6*).

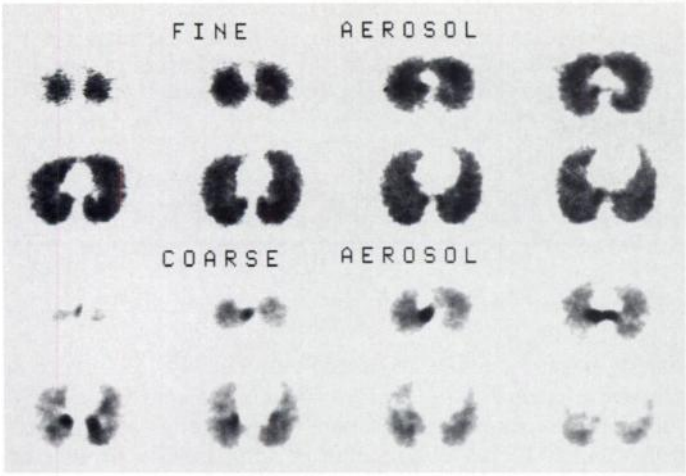


**FIGURE 2.** Transverse SPECT slices for both aerosols for one of the normal subjects. Each set of images is normalized to its own maximum.

### Comparison of Deposition Distribution from Two Nebulizers

SPECT and MRI of the pulmonary distribution of inhaled radiolabeled aerosol were performed on twelve normal male subjects as previously described. Permission was obtained from the local Ethics Committee and the Administration of Radioactive Substances Advisory Committee. Each subject was imaged twice following inhalation from two different nebulizers which produced aerosols of different mass median aerodynamic diameters (1.5 and 6.5 $\mu$m). These are subsequently described as the fine and coarse aerosols, respectively. The right lung SPECT data were hemispherically transformed and normalized to the total count in the right lung. The hemispherical data for all the subjects were then averaged for each aerosol. The polar plots and shell data were also averaged for each aerosol. A three-dimensional central to peripheral concentration ratio was derived as

$$R = \left( \sum_{i=1}^{3} s_i \Big/ \sum_{i=1}^{3} T_i \right) \Big/ \left( \sum_{i=8}^{10} s_i \Big/ \sum_{i=8}^{10} T_i \right). \qquad \text{Eq. 4}$$

The shell data were converted to distribution by generation and the conducting to alveolated airways concentration was calculated as:

$$A = \left( \sum_{j=1}^{14} g_j \Big/ \sum_{j=1}^{14} G_j \right) \Big/ \left( \sum_{j=15}^{23} g_j \Big/ \sum_{j=15}^{23} G_j \right). \qquad \text{Eq. 5}$$

A two-dimensional concentration ratio was also assessed (*2*). Each of the parameters was averaged for both aerosols and the significance of the difference calculated by the Wilcoxon matched pairs rank sum test.

## RESULTS

A typical set of transverse SPECT slices for one subject for both aerosols is shown in Figure 2. The average hemispherical plots are shown in Figure 3. The deposition concentration at the center of the hemisphere was higher for the coarse aerosol while the fine aerosol gave a more homogeneous distribution pattern. Both aerosols tended to have a relatively high concentration at the posterior base. Although this was the general pattern, considerable intersubject variation was observed. The corresponding mean polar plots of deposition for the two nebulizers are shown in Figure 4 along with those of the mean CT images. These images effectively summarize the three-dimensional data. The higher concentration of deposition of the coarse aerosol at the lung center and towards the posterior base of the

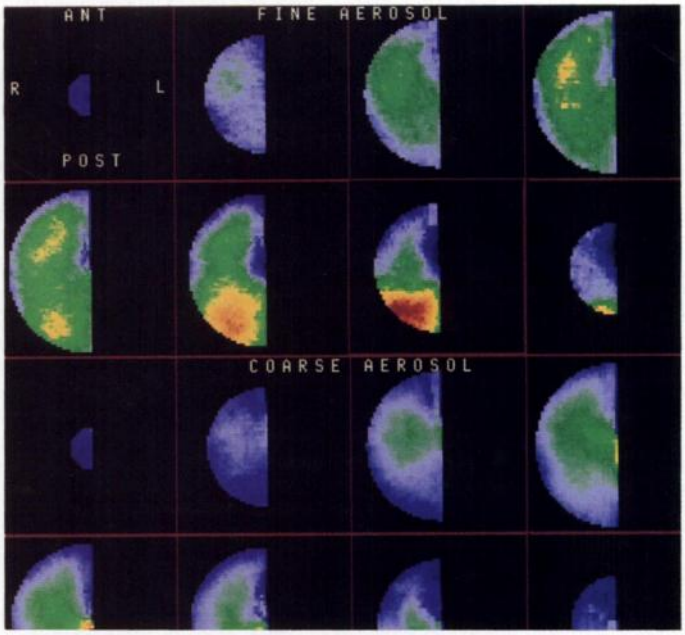


**FIGURE 3.** Mean hemispherical plots of deposition of both aerosols in the right lung displayed as a series of semicircular transverse slices. Slice orientation is indicated in the top left image. For each image set, the apex of the lungs is top left and the images then run successively down the lung moving left to right and then upper row to lower row.

lung coincided with higher density on the CT plot. The apparent increased density at the periphery resulted from the partial volume effect.

Figure 5 shows the variation of mean concentration with shell for both aerosols. The coarse had the expected higher concentration in the central shells. The mean three-dimensional central to peripheral concentration ratios for fine and coarse aerosols were 0.93 and 2.06, respectively. Figure 6 shows the mean deposition data for both aerosols converted to deposition per generation. For the coarse aerosol, the percentage per generation first decreased with the generation number but then increased due to the increasing volume of the outer generations. The fine aerosol had reasonably constant deposition per generation for the conducting airways (generation 1 to 14). For these generations, deposition of the fine aerosol was significantly lower than that of the coarse aerosol. The conducting to alveolated airway concentration ratios were 2.43 and 5.27 for the fine and coarse aerosols, respectively. The comparison of

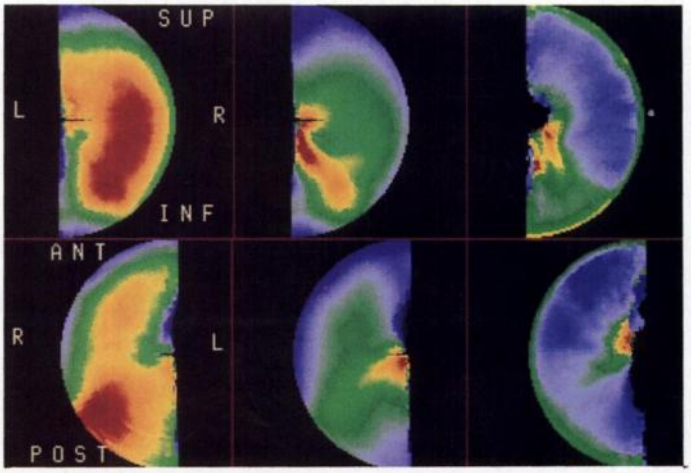


**FIGURE 4.** Coronal (top) and transverse (bottom) polar plots of deposition in the right lung of the fine aerosol (left) and the coarse aerosol (center) and for lung density from the CT images (right). Image orientation is indicated in the left image for each type of plot.

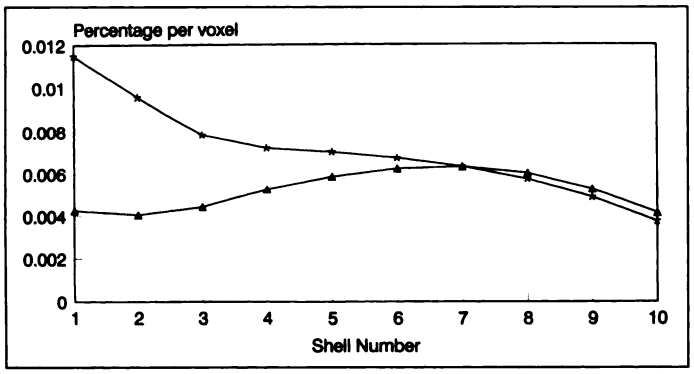


**FIGURE 5.** Variation of mean activity concentration per voxel with central to peripheral distance (shell number) for the fine (▲) and coarse (*) aerosols.

the various parameters for assessing the central to peripheral deposition concentration ratio is shown in Table 1. For all three parameters, there was a significant increase in the ratio between the values for the coarse and fine aerosol. For each aerosol, however, the estimates of the ratio were quite different when assessed by the different parameters. The mean percentage of total lung deposition in the conducting airways for both aerosols is also shown. Although there is a large difference in these values, both are small percentages of the total activity so that the percentage deposition in the acini differs relatively little between the aerosols, being over 90% in both cases.

The mean positional error in image alignment was 7.1 mm, of which a small component was due to the error in positioning the SPECT markers (1.5 mm). The qualitative effect of this degree of misalignment on the visual appearance of the hemispherical transform was negligible. The mean magnitude error on the concentration per shell was 2.5%.

## DISCUSSION

In this study, the combination of CT and MR data with SPECT has significantly enhanced the information available as compared to SPECT imaging alone. It has improved the accuracy of quantification of the distribution of activity and has enabled it to be localized with respect to the anatomy. The use of surface markers for alignment of internal organs has inherent limitations in accuracy. In this study, however, visual assessment of overlaid equivalent slices showed good alignment and deliberate misalignment by typical errors had minimal effect on the results.

The hemispherical transform proved a useful method of combining data on different subjects in a common format to enable the distribution pattern for a given administration protocol to be averaged and different protocols compared. It was helpful in studying inhaled particle deposition where information on penetration from center to periphery of the lung is of primary interest. The hemisphere could be divided into concentric shells to study the variation of deposition pattern with penetration. The model also allowed for summary of the data from three to two dimensions which enabled ready comparison of intersubject variation.

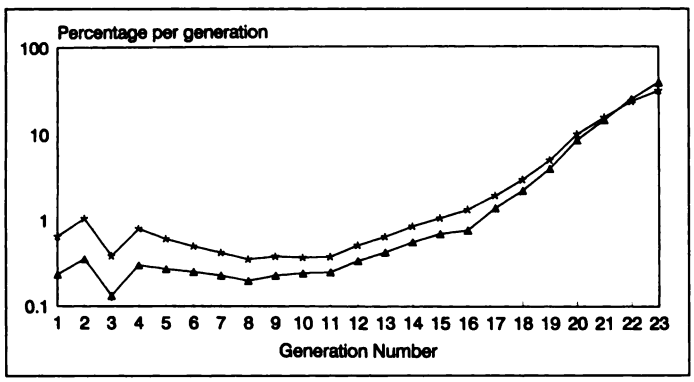


**FIGURE 6.** Mean total activity per airway generation expressed as a percentage of total lung activity for the fine (▲) and coarse (*) aerosols.

**TABLE 1**
Mean Values of Various Measures of Central-to-Peripheral Concentration Ratio of Pulmonary Aerosol Deposition and Percentage Pulmonary Deposition in Conducting Airways

| Aerosol | Two-dimensional ratio | Three-dimensional ratio (R) | Airway generation ratio (A) | Percentage deposition in conducting airways |
|---|---|---|---|---|
| Fine | 2.03 | 0.93 | 2.43 | 4.03 |
| Coarse | 2.61 | 2.19 | 5.27 | 7.84 |

The symmetrical nature of the hemispherical plot has also enabled it to be related to the symmetrical Weibel model of the lung. The spatial model of the airway tree allowed derivation of the aerosol deposition pattern in relation to its different generations. The deposition data was then in the form that is important to physicians using aerosol inhalation therapy in the treatment of asthma and other conditions. Information on the deposition pattern in the different airways will be of value in understanding the mechanisms of the action of drugs and in optimizing treatment regimens. It will also be valuable to computer modelers of aerosol deposition seeking validation of their models. The general shape of the curves showing deposition by generation for the two different particle sizes (Fig. 6) is similar to that obtained by modelers of clinically inhaled aerosols (*13*). A detailed comparison between our results with those of computer modeling and previous experimental work (*14*) will be the subject of further study.

The estimates of central to peripheral concentration ratio from planar and even SPECT spatial data are very different from those obtained for the central to alveolated airways (Table 1). Planar imaging underestimates the ratio due to the mixture of central and peripheral tissue in the central area, although this is somewhat counterbalanced by the fact that the thickness of lung tissue represented by each pixel is less for the peripheral region. The three-dimensional nature of the spatial ratio derived from SPECT clearly overcomes these problems. It also, however, underestimates the difference for two reasons: (a) central voxels contain a mixture of conducting and alveolated airways and (b) the volume of airways per unit space volume is reduced towards the center of the lung. In providing correction for both these effects, the ratio expressed by airway generation should in principle be the most accurate. No gold standard exists for validation of this data but the proposed comparison with computer modeling (*13*) and previous experimental data (*14*) will help to put the current results into context.

Analysis of the CT images enabled the spatial variation of lung density to be related to deposition distribution (Fig. 4). The higher density obtained centrally was expected as anatomical structure predicts a higher density for conducting airways compared to acini. This results from observations of lung casts which show that both arteries and veins follow a similar branching structure for the conducting airways generations (*4*). This provided further evidence that the higher deposition concentration of the coarse aerosol in these central locations was due to increased deposition in conducting airways. The higher density of tissue inferiorly and to a lesser extent posteriorly suggested a relatively high number of conducting

airways in these positions. This is consistent with understanding of lung anatomy and also helps to explain the increased deposition at these locations. The nonsymmetrical nature of the airways indicated by the CT images highlights the limitations of our current symmetrical model but also provides useful data for its future development.

## CONCLUSION

Hemispherical transform analysis has proved capable of enhancing the interpretation of data from multimodality imaging of the distribution of inhaled aerosol. Such data should be of value in inhalation therapy and computer modeling of deposition.

## ACKNOWLEDGMENTS

We thank Fisons U.K. and the Leverhulme Trust for their support for this study.

## REFERENCES

1. Agnew J. Characterizing lung aerosol penetration. *J Aerosol Med* 1991;4:237–249.
2. Phipps PR, Gonda I, Bailey D, Borham P, Bautovich G, Anderson SD. Comparisons of planar and tomographic scintigraphy to measure the penetration index of inhaled aerosols. *Am Rev Respir Dis* 1989;139:1516–1523.
3. Perring S, Summers Q, Fleming JS, Nassim MA, Holgate ST. A new method of quantification of the pulmonary regional distribution of aerosols using combined CT and SPECT and its application to nedocromil sodium administered by metered dose inhaler. *Br J Radiol* 1994;67:46–53.
4. Weibel ER. Design of airways and blood vessels considered as branching trees. In: Crystal RG, West JB, et al., eds. *The lung: scientific foundations*. New York: Raven Press; 1991;711–720.
5. Martonen TB, Yang Y, Hwang D, Fleming JS. Mapping the human lung using Delaunay tesselation. *Comp Biomed Res* 1994;27:245–262.
6. Fleming JS, Nassim MA, Hashish AH, et al. Description of pulmonary deposition of radiolabeled aerosol by airway generation using a conceptual three dimensional model of lung morphology. *J Aerosol Med* 1995;8:341–346.
7. Fleming JS, Britten AJ, Perring S, Keen AC, Howlett PJ. A general software system for the handling of medical images. *J Med Eng Tech* 1991;15:162–169.
8. Conway JH, Hashish A, Halson P, et al. The assessment of deposition of two types of nebulized aerosols in the lung via the use of single-photon emission computed tomography and magnetic resonance imaging. *Nucl Med Commun* 1994;15:261.
9. Swithenbank J, Beer JM, Taylor DS, Abbot D, McGreath GC. A laser diagnostic technique for measurement of droplet and particle size distribution. *Prog Astronautics Aeronautics* 1977;53:421–437.
10. Hill DLG, Hawkes DJ, Crossman JF, et al. Registration of MR and CT images for skull base surgery using point like anatomical features. *Br J Radiol* 1991;64:1030–1035.
11. Halson PM, Moore E, Fleming JS, Conway J. Quantitative analysis of pulmonary deposition by single-photon emission computed tomography and magnetic resonance imaging. *Br J Radiol* 1994;67(suppl):41.
12. Fleming JS. A technique for using CT images in attenuation correction and quantification in SPECT. *Nucl Med Commun* 1989;10:83–97.
13. Martonen TB, Katz I. Deposition patterns of polydisperse aerosols within human lungs. *J Aerosol Med* 1993;6:251–274.
14. Stahlhofen W, Rudolf G, James AC. Intercomparison of experimental regional aerosol deposition data. *J Aerosol Med* 1989;2:285–308.